# Multi-target Planar Needle Steering with a Bio-inspired Needle Design

**Christopher Burrows, Fangde Liu, Alexander Leibinger, Riccardo Secoli and Ferdinando Rodriguez y Baena**

**Abstract** Percutaneous intervention is common practice in many diagnostic and therapeutic surgical procedures. Needle steering research aims to extend these by enabling therapies that are not possible with a straight rigid needle. Being able to address multiple targets in one insertion is an example of such a therapy, which would result in reduced overall trauma to the patient and surgery time. However, needle steering remains challenging, as soft tissue is highly compliant and deformable, and thus difficult to interact with. In this work, we develop a new biologically inspired needle design (4 mm outside diameter) and show its capabilities in multiple moving target scenarios. In vitro results in gelatin demonstrate accurate 2D tracking of two virtual targets over 3 target movement rates.

**Keywords** Needle steering · Bio-inspired · Medical robotics

## 1 Introduction

One of the potential technologies for improving minimally invasive surgery is needle steering, with research in this area growing significantly in recent years. Needle steering technologies offer an alternative means of therapy compared to standard percutaneous intervention techniques. Using a flexible needle and typically a robotic system, a needle can be guided along a curved path within the tissue. This potentially enables therapies that would otherwise not be available with a straight line path, for example steering around a critical region in the tissue, and alternative treatments for multiple lesions which could be accessed through a single insertion. Also, as the needle is able to steer, the trajectory of the needle can be adjusted in situ to compensate for moving targets due to the soft tissue deforming, as to reduce the final positional error and the need for reinsertion in the event that the target is missed. Being able to address multiple targets, such as in brachytherapy of the prostate, during one needle insertion is beneficial to the patient, as reducing the number of insertions results

C. Burrows · F. Liu · A. Leibinger · R. Secoli · F. Rodriguez y Baena (✉)
Imperial College, London, UK
e-mail: f.rodriguez@imperial.ac.uk

in decreased tissue trauma. This, in turn, minimizes recovery time and stress for the patient, while, from a surgical standpoint, this technique also reduces overall surgery time and cost.

Within this context, we aim to develop a steerable needle for the specific purpose of multi-target percutaneous access. Several needle steering technologies have been developed in order to produce curvilinear paths within tissue; however, these designs have drawbacks that make them unsuitable for certain clinical scenarios. For example, concentric tube based needle systems operate well inside a cavity but suffer from important kinematic constraints when used percutaneously [4, 12]. Bevel and kinked tip needle steering systems are accurate and have a good range of possible curvatures, but the needle must be rotated as it is inserted, causing additional trauma to the surrounding tissue [11] although in some tissues and scenarios this effect may be negligible [9]. In light of these weaknesses, our group has developed a flexible needle controlled using a biologically inspired multi-segment design [6]. Our Soft Tissue Intervention and Neurosurgical Guide (STING) has a unique actuation mechanism which employs a 'programmable bevel' in order to steer along arbitrary curvilinear paths. Recent prototypes produced by this research that have been published in the literature are a two segment needle prototype, with a 4 mm outer diameter (OD), which is capable of only planar steering, and a four segment needle prototype, with an 8 mm OD, capable of 3D steering but not of a clinically acceptable size. This paper describes the design and manufacture of a new four segment, 4 mm OD needle and its application to multi-target delivery. Our group has previously developed a system for reaching a single moving target, with on-line path planning on a plane [2]. Here, we describe the extension of this on-line path replanner to multiple moving targets and use it to assess the performance of the new needle design in vitro.

This paper is structured as follows: Sect. 2 presents the new needle design and Sect. 3 describes how the control system was developed to reach multiple targets. Sections 4 and 5 present the validation experiments performed to assess the system and a discussion of the results, respectively. Finally, Sect. 6 presents conclusions and future work.

## 2 Needle Design

In this work, we continue to miniaturize the STING needle toward a size that is realistic for clinical applications. The latest prototype prior to this work was a two segment needle prototype, 4 mm OD, only capable of planar steering [6]. Here, we present a new, four segment needle design, of the same OD, shown in Fig. 1. This needle is the first prototype of this size that is capable of steering in 3D, due to the four segment design. This was achieved by pushing the boundaries of the additive layer manufacturing technique used in this work. As with all of the previous designs, this needle was produced using rapid prototyping technology (Objet Connex, Stratasys Ltd.) however, a novel approach was required in order to produce a four segment needle at this scale.
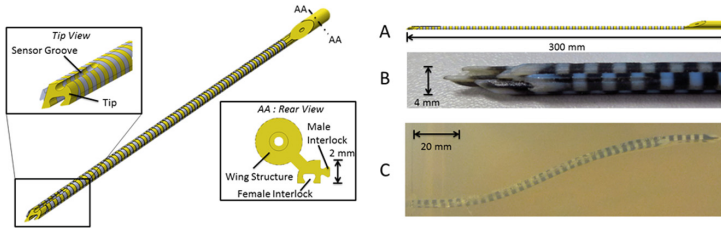
**Fig. 1** 3D render (*Left*) and side profile (*A*) of one of the segments of the new STING needle prototype, showing the wing and tip designs and the 'composite' body structure made up of soft (*black*) and rigid (*white*) sections. Picture of the needle tip (*B*) and the new needle performing a double bend trajectory (*C*)

The principal shape of the needle remains the same as in previous versions [1], with four 'dovetail' interlocked segments that can slide independently of each other; a 3D model of one of the segments and the assembled needle is shown in Fig. 1. The needle has a wing structure similar to the design in [6], which allows the needle to be actuated from the back. The cross section of the segments was optimized using the technique described in [7], where several parameters of the needle design are adjusted to create an interlock optimized against two failure modes. The cross section and wing structure can be seen in Fig. 1 AA: Rear View. The length of the needle is 300 mm and the tip of the needle is made of VeroWhitePlus (Stratasys Ltd.). A groove is present at the tip so that an electromagnetic sensor (Northern Digital Inc.) can be attached, to allow translational and rotational tracking of the needle tip during insertion.

The body of this design is made up of a 'composite' structure, with alternating rigid and soft sections, as shown in Fig. 1B. The soft sections are made from FLX9885 (Stratasys Ltd.) and the rigid sections VeroWhitePlus (Stratasys Ltd.). This 'composite' structure is required since, at the required dimensions, the interlock strength is not high enough to prevent the needle from failing due to the segments coming apart. The alternating structure prevents the smaller dimension dove-tail interlocking mechanism between segments from failing, [7], with the rigid sections along the length of the body in both the male and female sections adding strength to the interlocking mechanism. The soft regions interspersed between the rigid sections allow the prototype to remain flexible and able to bend.

## 3 Controlling to Multiple Targets

An on-line path planner based needle steering system developed to reach a moving target was first demonstrated in [2]. This planner produces locally optimal smooth continuous paths and can also constrain the curvature and the gradient of curvature
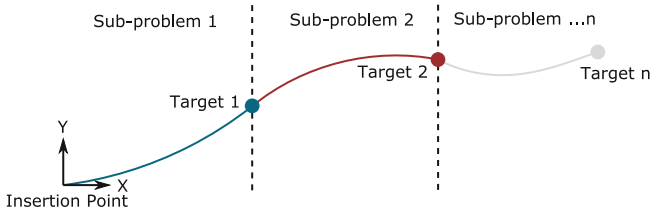
**Fig. 2** Diagram of the process carried out by the planning system. Given *n* targets, each target is considered individually and sequentially and therefore, as a sub-problem. Upon reaching a target, the next target in the sequence is considered and this continues until all the targets have been reached

of the path online during an insertion. Here, this system is extended so that multiple targets can be addressed within one insertion.

To allow multiple targets to be reached, the overall plan that connects all of the targets is broken down into sub-objectives. Specifically, the path between the targets is divided up into *n* sub-problems, *n* being equal to the number of targets. This is shown in Fig. 2, where each target is considered sequentially ($i = 1, 2, ...n$) in its local frame, as separate control sub-problems which are iterated through. Currently, the system is limited to sub-problems where the direction of the curvature of the path between the current needle state and target remains the same. This requirement can be met by setting suitable constraints in the global pre-planner of the needle steering system, see [2] for more details. The direction of curvature to the target in the current sub-problem is determined from the local needle frame and the associated approach angle of each target (set from the pre-planner in the initial phase).

The algorithm from [2] is then used to replan the path between the needle and the target pose in each sub-problem as the target moves. This has the advantage that the replanning system used for the single moving target can be added into the multi-targeting system with little modification. The result of this system is that locally optimal paths (the shortest path that satisfies the constraints) for each target are produced, as the surgical scenario changes dynamically, under the effect of tool-tissue interactions.

## 4 In Vitro Testing

### 4.1 Experimental Setup

The experimental setup used to test the needle steering system is similar to that used in previous experiments [2, 6]. The actuation method for moving the needle consists of a set of linear actuators, motor driven lead screws connected to the needle by nitinol push rods, controlled via a CompactRIO controller programmed with

**Table 1** Experimental parameters

| Parameter | Symbol | Value |
|---|---|---|
| **Preplan** [6] | | |
| Start state | $[x, y, \theta, \rho]$ | [0,0,0,0] |
| Max. curvature (mm$^{-1}$) | $\rho_{max}$ | 0.01 |
| Max. deriv. curvature (mm$^{-2}$) | $\dot{\rho}_{max}$ | $7.80 \times 10^{-4}$ |
| **Controller** [5] | | |
| Compensation coefficient | $\varepsilon$ | 2.4 |
| Steering coefficient (mm$^{-2}$) | $\kappa$ | $3.90 \times 10^{-4}$ |
| Max. steering offset (mm) | $\delta_{max}$ | 30 |
| Sampling time (s) | $T_p$ | 2 |
| Subsampling time (s) | $T_s$ | 0.25 |
| Prediction horizon | $N_p$ | 10 |
| Subsample prediction horizon | $N_s$ | 8 |
| **Deformation planner** [2] | | |
| Target movement threshold (mm) | $D_{max}$ | 0.2 |
| Number of segments | $n_{seg}$ | 10 |
| Max. curvature (mm$^{-1}$) | $\rho_{max}$ | 0.01 |
| Max. deriv. curvature (mm$^{-2}$) | $\dot{\rho}_{max}$ | $7.80 \times 10^{-4}$ |

LabVIEW (National Instruments Corp.). The control system, as described in Sect. 3, was implemented in C++ and python. The controller for the needle, a MPC-based approach [5], was implemented in C++ using Quadprog++ as the quadratic programming solver. The Deformation planner was implemented using python (2.7) and the CVXOPT optimization library. An EM tracking sensor (Aurora 5 DOF sensor with 0.5 mm diameter and 8 mm length, Northern Digital Inc.), with a root-mean-square (RMS) accuracy of 0.7 mm, was attached to the sensor groove of one of the segments to measure the position of the needle tip. Bovine gelatin, 250 bloom (Sleaford Quality Foods, Sleaford, UK), 4.5 wt%, was used as the tissue phantom in the experiments, with a Young's modulus, $E = 7$ kPa. The parameters used for the control system are shown in Table 1.

## 4.2 Segment Offset Versus Curvature Calibration

Before determining the performance of the system, the needle prototype's steering performance was evaluated. Experiments with the new needle design were performed to ascertain the coefficient between segment offset and resultant path curvature, $\kappa$. It was previously shown that this coefficient is approximately linear [1, 5] and can be used to control the needle along curved trajectories by controlling segment

offset. Six insertion tests [1], with a constant steering offset between the segments ($\delta$) of 5–30 mm (in 5 mm increments) were carried out, with the EM tracking system used to track the needle tip path, with a resulting $\kappa = 3.89 \times 10^{-4}$ mm$^{-2}$. With this linear coefficient, an offset of 25.7 mm would be required to produce a radius of curvature of 100 mm.

## *4.3 Experimental Scenarios*

To evaluate the new needle design's ability to reach multiple moving targets, two scenarios were designed. The scenarios consist of guiding the needle to two moving virtual point targets that have varying degrees of target movement, as follows: (1) Two targets moving within the plane requiring curvature in a single direction, known as **2-Tar-SB**; (2) Two targets moving within the plane requiring a change in curvature direction after the first target (inflection point, S-Curve), known as **2-Tar-DB**. Each target has an associated 2D pose (x, y, approach angle) that the controller tries to drive the needle to. For **2-Tar-SB** the target poses were (100 mm, 20 mm, 27.4°) and (160 mm, 60 mm, 42.9°) respectively. For **2-Tar-DB** the target poses were (80 mm, 15 mm, 24.3°) and (160 mm, 42 mm, 7.8°) respectively. These target poses were chosen as they are near the edge of the needle workspace and therefore close to the constraint limits.

In order to test the system, the range of total displacements was chosen that matched the tissue values found in published studies [3, 8]. Three constant movement rates small (0.015 mm/s), medium (0.025 mm/s), large (0.05 mm/s) for the target displacements were then based on these values. The virtual target movement is then computed as a combination (sum) of two vectors. The constant movement vector, defined above, acts in the direction of the initial insertion axis of the needle. The second vector then acts in the direction of the tip axis with a rate of 0.075 mm/s when less than 20 mm away from the target. This is to simulate the deformation, in a simplified manner, seen from inserting the needle into soft tissue [10].

## 5   Results and Discussion

Each of the scenarios described in Sect. 4.3 was performed three times with each of the virtual target movement rates, resulting in a total of eighteen experiments.

Figure 3a and b show example results from **2-Tar-SB** and **2-Tar-DB** respectively. The tip position and angle error to each target was calculated for all the experiments. Across all movement rates, the mean positional errors for Target 1 and 2 were 0.3 mm and 0.6 mm, with SDs of 0.15 mm and 0.31 mm respectively. The positional error averaged over all targets and experiments was 0.46 mm with an SD of 0.17 mm.
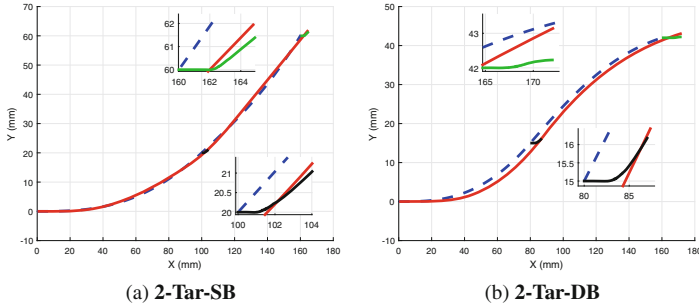
**Fig. 3** Results from the experiments showing the performance in reaching two moving virtual targets: Initial path (*blue dashed*), smoothed needle path (*red*), and target paths (*black* for Target 1 and *green* for Target 2) with a large target movement rate. Insets show details of Target 1 (*bottom*) and Target 2 (*top*) paths

Across all movement rates, the mean approach angle errors for Target 1 and Target 2 were 1° and 1.1°, with SDs of 1.02° and 1.83° respectively. The approach angle error averaged over all targets and experiments was 1.05°, with an SD of 0.32°.

The results in Table 2 show that the new needle design is capable of similar steering performance to the two part needle of equal cross section, described in [6], where the mean targeting error was 0.51 mm and SD 0.85 mm. Additionally, the maximum bending performance was 19.4 % worse than that obtained for the 2-part prototype [6], which had an offset coefficient $\kappa = 4.824 \times 10^{-4}$ mm$^{-2}$. This can be explained by the fact that, compared to the previous design, the new design is symmetrical, has rigid sections along the length of the body, and has more material in its cross section (greater bending stiffness) due to the interlock design and lack of working channel. Further refinement of this design will also improve steering performance. For both scenarios, qualitative analysis shows, the target position error increases for Target 2, as shown by the increase in total mean. This is likely due to the increased insertion length and therefore increased overall target displacement compared to Target 1, however this does not appear to be linked to the Target movement rate as the mean position error values for Target 2 are within a similar range across all the scenarios.

These results demonstrate that the new needle design used in this work can be used within a needle steering system and guided towards multiple moving targets in plane, across a range of movement rates, under path constraints (curvature and its derivative), with small position and angular errors. The rate of movement of the targets does not appear to affect the ability of the system to guide the needle to the target position, with all the errors within a similar range.

**Table 2** Positional and angular error results

| Scenario | Deformation | Target 1—Positional error (mm) | | Target 1—Angle error (Deg.) | | Target 2—Positional error (mm) | | Target 2—Angle error (Deg.) | |
|---|---|---|---|---|---|---|---|---|---|
| | | Mean | SD | Mean | SD | Mean | SD | Mean | SD |
| 2-Tar-SB | Small | 0.28 | 0.21 | 1.38 | 0.57 | 0.79 | 0.32 | 1.38 | 0.74 |
| | Medium | 0.23 | 0.17 | 0.69 | 1.15 | 0.53 | 0.21 | 1.09 | 2.86 |
| | Large | 0.39 | 0.12 | 1.2 | 0.60 | 0.63 | 0.62 | 0.69 | 1.09 |
| 2-Tar-DB | Small | 0.30 | 0.24 | 1.20 | 0.8 | 0.36 | 0.17 | 0.74 | 1.15 |
| | Medium | 0.33 | 0.15 | 0.69 | 0.70 | 0.71 | 0.22 | 1.72 | 3.40 |
| | Large | 0.43 | 0.06 | 0.86 | 2.29 | 0.57 | 0.33 | 0.97 | 1.71 |
| | Total mean | 0.30 | 0.15 | 1.00 | 1.02 | 0.60 | 0.31 | 1.11 | 1.83 |

# 6 Conclusion and Future Work

This paper describes our latest work in developing a novel steerable needle for percutaneous intervention. A new 4 mm four-part, 3D steering capable, prototype with a novel 'composite' structure was developed. The new needle design was then tested experimentally by using an extension of an online path planner to guide the needle to two virtual moving targets over various scenarios. The experimental results showed a mean positional error of 0.46 mm and approach angle error of 1.05° over 18 experiments. This work sets significant scope for future improvements. The natural progression of this work is an extension to 3D, with the development of a controller and planning algorithm capable of following arbitrary trajectories across all three planes. Development of the needle designs will continue, with the OD of the needle reduced further, by exploring alternative manufacturing techniques.

# References

1. Burrows C, Secoli R, Rodriguez y Baena F (2013) Experimental characterisation of a biologically inspired 3d steering needle. In: 2013 13th International conference on control, automation and systems (ICCAS). IEEE, pp 1252–1257
2. Burrows C, Liu F, Rodriguez y Baena F (2015) Smooth on-line path planning for needle steering with non-linear constraints. In: 2015 IEEE/RSJ international conference on intelligent robots and systems (IROS), pp 2653–2658. doi:10.1109/IROS.2015.7353739
3. Deurloo EE, Gilhuijs KG, Kool LJS, Muller SH (2001) Displacement of breast tissue and needle deviations during stereotactic procedures. Invest Radiol 36(6):347–353
4. Dupont PE, Lock J, Itkowitz B, Butler E (2010) Design and control of concentric-tube robots. IEEE Trans Robot 26(2):209–225
5. Ko SY, Rodriguez y Baena F (2012) Trajectory following for a flexible probe with state/input constraints: an approach based on model predictive control. Robot Auton Syst 60(4):509–521
6. Ko SY, Rodriguez y Baena F (2013) Toward a miniaturized needle steering system with path planning for obstacle avoidance. IEEE Trans Biomed Eng 60(4):910–917
7. Leibinger A, Oldfield M, Rodriguez y Baena F (2014) Multi-objective design optimization for a steerable needle for soft tissue surgery. In: The 15th international conference on biomedical engineering. Springer, pp 420–423
8. Lobo JR, Moradi M, Chng N, Dehghan E, Morris WJ, Fichtinger G, Salcudean SE (2012) Use of needle track detection to quantify the displacement of stranded seeds following prostate brachytherapy. IEEE Trans Med Imaging 31(3):738–748
9. Majewicz A, Marra S, van Vledder M, Lin M, Choti M, Song D, Okamura A (2012) Behavior of tip-steerable needles in ex vivo and in vivo tissue. IEEE Trans Biomed Eng 59(10):2705–2715. doi:10.1109/TBME.2012.2204749
10. Oldfield M, Burrows C, Kerl J, Frasson L, Parittotokkaporn T, Beyrau F, Rodriguez y Baena F (2014) Highly resolved strain imaging during needle insertion: results with a novel biologically inspired device. J Mech Behav Biomed Mater 30:50–60

11. Swaney PJ, Burgner J, Gilbert HB, Webster RJ (2013) A flexure-based steerable needle: high curvature with reduced tissue damage. IEEE Trans Biomed Eng 60(4):906–909
12. Webster RJ, Jones BA (2010) Design and kinematic modeling of constant curvature continuum robots: a review. Int J Robot Res